



Influence of nickel addition on structural and magnetic properties of aluminium substituted Ni-Zn ferrite nanoparticles

Donta Paramesh¹, Katrapally Vijaya Kumar^{2,*}, Pendyala Venkat Reddy¹

¹Sreenidhi Institute of Science and Technology (Autonomous), Ghatkesar, Hyderabad - 501301, Telangana State, India

²Department of Physics, Jawaharlal Nehru Technological University Hyderabad College of Engineering, Jagtial, Nachupally (Kondagattu), District: Karimnagar - 505501, Telangana State, India

Received 1 May 2016; Received in revised form 28 June 2016; Accepted 16 September 2016

Abstract

Ni-Zn-Al mixed ferrite nanoparticles, with general formula $Ni_xZn_{1-x}AlFeO_4$ ($x = 0.0, 0.2, 0.4, 0.6, 0.8$ and 1.0), were synthesized by sol-gel auto combustion technique. All prepared ferrite nanoparticles were characterized by X-ray diffraction, scanning electron microscopy, energy dispersive X-ray spectroscopy, Fourier transform infrared spectroscopy and vibrating sample magnetometer. X-ray diffraction study confirmed the formation of the single phase cubic spinel structure in all ferrite samples. The crystallite size was calculated by the Debye-Scherrer formula and found to be in the range 15–46 nm. The lattice constant decreased with increasing Ni^{2+} ion concentration. Scanning electron microscopy images clearly indicate that the particles are very small but agglomerated. Energy dispersive X-ray was used to confirm the composition of the prepared powders. Fourier transform infrared spectra showed two main absorption bands of ferrite nanoparticles, the high frequency band (ν_1) around 600 cm^{-1} and the low frequency band (ν_2) around 400 cm^{-1} arising from tetrahedral (A) and octahedral (B) interstitial sites in the spinel lattice, respectively. Vibrating sample magnetometer results reported that the saturation magnetization, remanent magnetization and magnetic moments decrease with increasing Ni^{2+} ion concentration.

Keywords: Ni-Zn-Al ferrite nanoparticles, sol-gel auto combustion technique, structure, magnetic properties

I. Introduction

The mixed spinel nano-ferrites have a wide range of applications in the various fields of science and technology. Various ferrite preparation techniques, doping and cation substitutions play an extraordinary role in deciding and controlling the characteristics of nano-ferrite particles. Substituting the trivalent and pentavalent ions gives rise to many applications of ferrites in different areas such as magnetic storage, transformer cores, magnetic cards, magnetic recording, permanent magnets, computer peripherals, electronic devices, microwave devices and catalysts. Ferrites have high electrical resistivity and low eddy current losses, consequently they are well suitable for high frequency applications [1–8]. Normally, in ferrites nickel has a strong tendency to occupy the octahedral sites whereas zinc

occupies the tetrahedral site. Thus, nickel ferrite has an inverse spinel structure whereas zinc ferrite has a normal spinel structure. Hence, Ni-Zn ferrites have a mixed spinel ferrite structure and are used as a wave absorber for electromagnetic interference [9]. The tetrahedral sites are occupied by Zn^{2+} and Fe^{3+} whereas the octahedral sites are occupied by Ni^{2+} and Fe^{3+} . The interactions between the ions in tetrahedral and octahedral sites can alter magnetic and electrical properties of nano-ferrites. The ferrite properties are also highly dependent on the methodology adopted for their synthesis, preparative conditions, sintering temperature and time, chemical composition, grain size etc. [10–12].

Presently, we have chosen the sol-gel auto combustion technique to prepare the ferrite composition of $Ni_xZn_{1-x}AlFeO_4$ ($x = 0.0, 0.2, 0.4, 0.6, 0.8$ and 1.0) and investigate the influence of Ni:Zn ratio on their structure and magnetic properties. The addition of Al^{3+} ions alters the distribution of the ions in the spinel ferrite struc-

*Corresponding author: tel: +91 900 0203797, e-mail: kvkphd@gmail.com

ture. Usually the Al^{3+} ions occupy octahedral sites and increase the strength of metal–oxygen bond by replacing larger ionic radii Fe^{3+} ions in the octahedral sites.

II. Experimental

$\text{Ni}_x\text{Zn}_{1-x}\text{AlFeO}_4$ ($x = 0.0, 0.2, 0.4, 0.6, 0.8$ and 1.0) ferrite nanoparticles were prepared from chemical reagents with analytical grade (AR) and $>99\%$ of purity. The used precursors were zinc nitrate hexahydrate - $\text{Zn}(\text{NO}_3)_2 \cdot 6\text{H}_2\text{O}$ (AR), nickel nitrate - $\text{Ni}(\text{NO}_3)_2 \cdot 6\text{H}_2\text{O}$ (AR), aluminium nitrate nonahydrate - $\text{Al}(\text{NO}_3)_3 \cdot 9\text{H}_2\text{O}$ (GR), ferric nitrate - $\text{Fe}(\text{NO}_3)_3 \cdot 9\text{H}_2\text{O}$ (GR) and citric acid monohydrate - $\text{C}_6\text{H}_8\text{O}_7 \cdot \text{H}_2\text{O}$ (GR). Citric acid is a chelating agent and fuel for self-combustion, but also helps for the homogenous distribution and separation of the metal ions. The ammonia was used to adjust pH value and improve the solubility of the metal ions.

Metal nitrates were taken in the required stoichiometric ratio and dissolved in a sufficient amount of double distilled water. The citric acid was added to the nitrate solution in 3:1 molar ratio. Further, the liquid ammonia was added to this nitrate solution drop by drop with constant stirring to maintain the pH value at 7. The resulting solution was constantly heated on the magnetic stirrer at 300°C to allow the gel formation. The resultant gel was kept in open air environment to remove the absorbed water and the precursor powder was calcined under the constant heating condition at 600°C for 5 hours to get the final product. The resultant powder was then ground into fine particles by an agate mortar and pestle.

Phase composition was studied by Rigaku X-ray diffractometer (Rigaku Miniflex II) using the CuK_α radiation ($\lambda = 1.5406 \text{ \AA}$). Scanning electron microscopy (SEM) images were obtained using a TESCAN, MIRA

II LMH microscope. The composition was determined by energy dispersive X-ray spectroscopy (EDX, Inca Oxford, attached to the SEM). FTIR analysis was carried out by FT/IR-4000, JASCO, Japan in the range $400\text{--}4500 \text{ cm}^{-1}$ at room temperature. Magnetic properties were studied by vibrating sample magnetometer (Lakeshore VSM 718 model) at room temperature.

III. Results and discussion

3.1. XRD analysis

The structural analysis of $\text{Ni}_x\text{Zn}_{1-x}\text{AlFeO}_4$ ($x = 0.0, 0.2, 0.4, 0.6, 0.8$ and 1.0) ferrite nanoparticles calcined at 600°C was performed by powder XRD method. Figure 1 shows the X-ray diffraction patterns of all prepared ferrite nanoparticles and confirm their crystalline structure with single phase spinel phase. The average crystallite size of the ferrite nanoparticles was calculated using the Debye-Scherrer equation [13,14]:

$$t = \frac{0.9\lambda}{\beta \cdot \cos \theta} \quad (1)$$

where, λ is wavelength of the X-ray radiation, β is full width at half maximum, θ is Bragg's angle. It was found that the average crystallite size of the ferrite nanoparticles is in the range $15\text{--}46 \text{ nm}$. It was noticed that the crystallite size and lattice constant gradually decreased with increasing Ni^{2+} ion concentration (Table 1). Decrease in the crystallite size and lattice constant may be due to the substitution of larger Zn^{2+} ions (0.84 \AA) with smaller Ni^{2+} ions (0.74 \AA) [15–18]. The lattice constant (a), X-ray density (ρ_X), bulk density (ρ_B), porosity and jump lengths (L_A, L_B) were determined by the equations (2), (3), (4), (5), (6) and (7), respectively (and listed in Table 1).

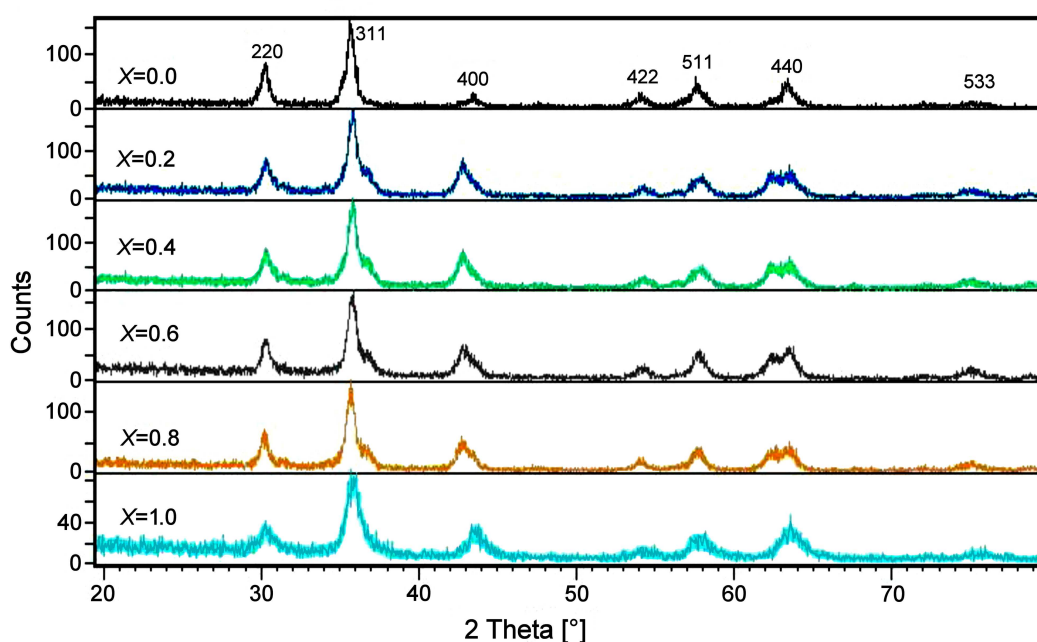


Figure 1. X-ray diffraction pattern of $\text{Ni}_x\text{Zn}_{1-x}\text{AlFeO}_4$ ($x = 0.0, 0.2, 0.4, 0.6, 0.8$ and 1.0) ferrite nanoparticles

Table 1. Lattice constant (a), X-ray density (ρ_X), bulk density (ρ_B), porosity, crystallite size - XRD (d_{XRD}), tetrahedral and octahedral jump lengths (L_A & L_B), tetrahedral frequency (ν_1), octahedral frequency (ν_2) of $Ni_xZn_{1-x}AlFeO_4$ ($x = 0.0, 0.2, 0.4, 0.6, 0.8$ and 1.0) ferrite nanoparticles

Composition (x)	a [Å]	ρ_X [g/cm ³]	ρ_B [g/cm ³]	Porosity [%]	d_{XRD} [nm]	L_A [Å]	L_B [Å]	ν_1 [cm ⁻¹]	ν_2 [cm ⁻¹]
0.0	8.334	4.869	3.784	22.28	46	3.609	2.946	634	411
0.2	8.327	4.850	3.893	20.22	46	3.605	2.944	635	409
0.4	8.314	4.842	3.905	19.35	41	3.600	2.939	634	414
0.6	8.307	4.824	3.947	18.18	34	3.597	2.937	631	404
0.8	8.295	4.814	3.981	17.30	21	3.592	2.933	636	413
1.0	8.281	4.807	3.997	16.85	15	3.586	2.927	605	414

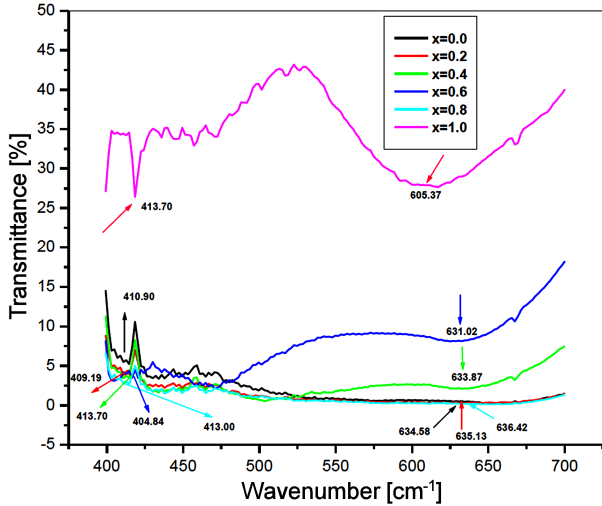


Figure 2. FTIR spectra of $Ni_xZn_{1-x}AlFeO_4$ ($x = 0.0, 0.2, 0.4, 0.6, 0.8$ and 1.0) ferrite nanoparticles

$$a = d \sqrt{h^2 + k^2 + l^2} \quad (2)$$

where, d is interplanar distance, $h k l$ are Miller indices.

$$\rho_X = \frac{8M}{N \cdot a^3} \quad (3)$$

where, M is molecular weight, N is Avogadro number, a is lattice constant.

$$\rho_B = \frac{m}{\pi \cdot r^2 \cdot t} \quad (4)$$

where, m is mass of the circular pellet, r is radius of the pellet, t is thickness of the pellet.

$$P = 1 - \frac{\rho_B}{\rho_X} \quad (5)$$

where, ρ_B is bulk density and ρ_X is X-ray density.

$$L_A = \frac{\sqrt{3}}{4}a \quad (6)$$

$$L_B = \frac{\sqrt{2}}{4}a \quad (7)$$

From Table 1 it was observed that the X-ray density and porosity decreased, bulk density increased with increasing Ni^{2+} ion concentration. In general, the X-ray density of nano-ferrites is higher than bulk density due

to existence of pores in the samples. The X-ray density depends on the molecular weights of the samples and lattice constants. The molecular weights of the prepared $Ni_xZn_{1-x}AlFeO_4$ samples were found to decrease from 212.15 to 205.46 g/mol by varying the composition. Hence, the X-ray density decreased as Ni^{2+} ion concentration increased [19]. The bulk density and porosity was inversely related with each other. Hence, the bulk density increased and the porosity progressively decreased with the increase of Ni^{2+} ion concentration (Table 1), which has already been observed in literature [20]. Jump length for A-sites and B-sites were found to decrease slightly with increasing Ni^{2+} ion concentration. This shows that less energy is required for jumping of electrons between A and B-sites as a result of which the conductivity increases. Jump lengths are directly related with lattice constants. So decrease of the lattice constant values consequently decrease the jump lengths.

3.2. FTIR study

Fourier transform infrared spectra of $Ni_xZn_{1-x}AlFeO_4$ ($x = 0.0, 0.2, 0.4, 0.6, 0.8$ and 1.0) ferrite nanoparticles calcined at 600 °C (Fig. 2) show the strong absorption bands with two characteristic peaks [21–24]. In ferrites the metal ions are situated at two sub-lattices named tetrahedral (A) site and octahedral (B) site. The high frequency tetrahedral (ν_1) band was observed in the range of 605–636 cm^{-1} and low frequency octahedral band (ν_2) was observed in the range of 404–414 cm^{-1} . These bands confirm the spinel structure of the prepared ferrite nanoparticles. Similar reports were published by Zahi and Pathak [25,26].

3.3. SEM and EDX analysis

Scanning electron morphologies of $Ni_xZn_{1-x}AlFeO_4$ ($x = 0.0, 0.2, 0.4, 0.6, 0.8$ and 1.0) ferrite nanoparticles calcined at 600 °C were shown in Fig. 3. It is clearly noticed that powder particles are in nano-size range and have high tendency to join together and form spherically shaped agglomerates [27,28]. Figure 4 shows the EDX images of all $Ni_xZn_{1-x}AlFeO_4$ ($x = 0.0, 0.2, 0.4, 0.6, 0.8$ and 1.0) ferrite nanoparticles calcined at 600 °C. The characteristic peaks of Ni, Zn, Al, Fe and O elements were observed in EDX spectra. Hence, the EDX patterns and the corresponding data in Table 2 confirm the presence of all constituting elements in the prepared ferrite nanoparticles [29].

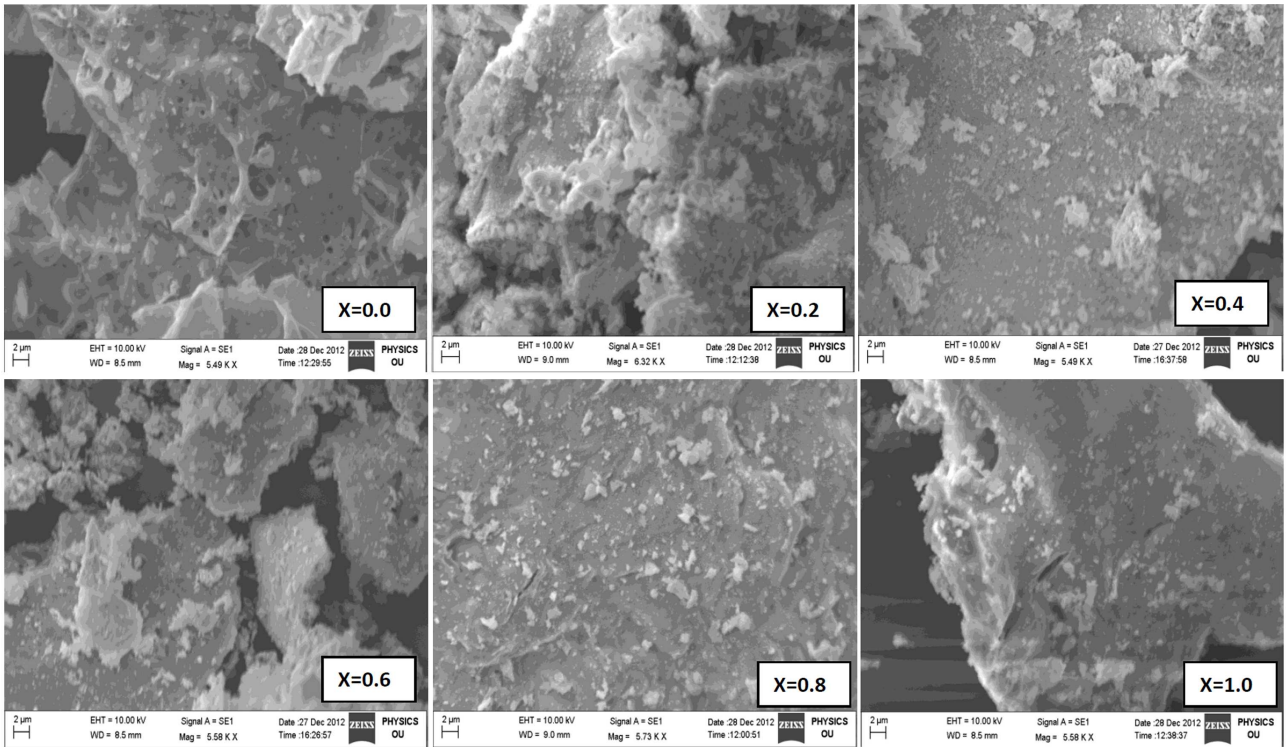


Figure 3. SEM images of $Ni_xZn_{1-x}AlFeO_4$ ($x = 0.0, 0.2, 0.4, 0.6, 0.8$ and 1.0) ferrite nanoparticles

3.4. Magnetic properties

The magnetic properties of ferrites were influenced by various parameters like anisotropy, crystallite size, density, composition and super exchange interactions between A and B-sites. Magnetic hysteresis loops of $Ni_xZn_{1-x}AlFeO_4$ samples calcined at $600^\circ C$ were obtained at room temperature by vibrating sample magnetometer and are shown in Fig. 5. The magnetic properties like saturation magnetization, remanent magnetization, coercivity and magnetic moments were elucidated from hysteresis loops and given in Table 3. From Table

3 it can be observed that all prepared ferrite nanoparticles show the soft and ferrimagnetic behaviour. The magnetic moment (μ_B) was calculated by the saturation magnetization and molecular weight of the prepared nanoferrite samples by equation [30]:

$$\mu_B = \frac{M_S \times M}{5585} \quad (8)$$

where M_S is saturation magnetization, M is molecular weight of a sample.

The magnetic hysteresis data confirmed that the satu-

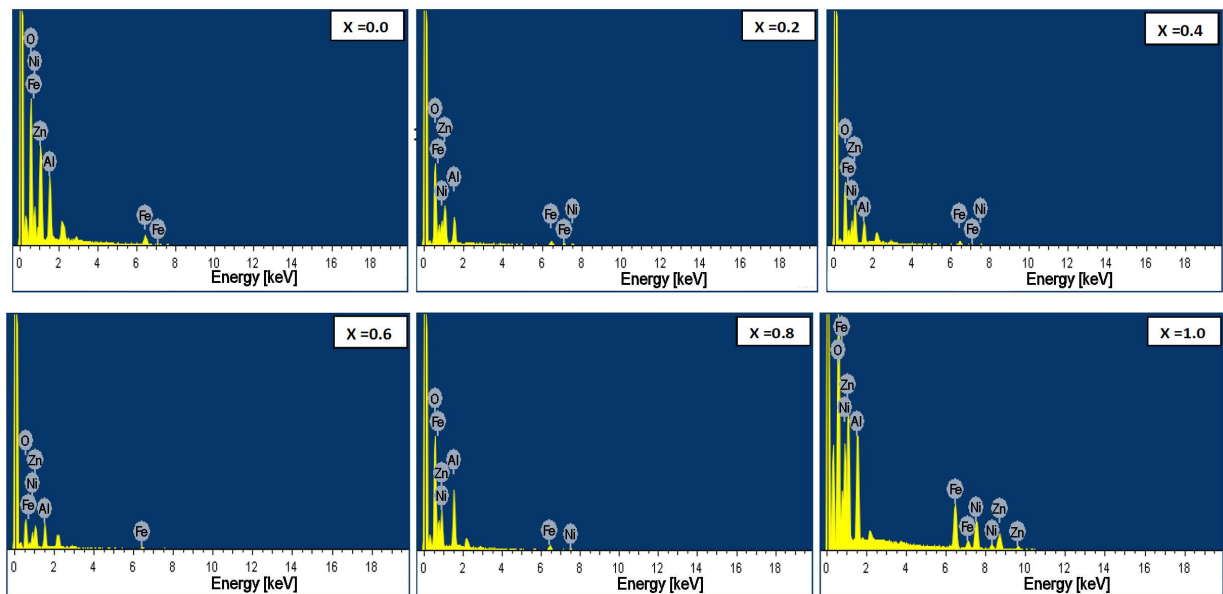


Figure 4. EDX pattern of $Ni_xZn_{1-x}AlFeO_4$ ($x = 0.0, 0.2, 0.4, 0.6, 0.8$ and 1.0) ferrite nanoparticles

Table 2. Elemental composition of Ni_xZn_{1-x}AlFeO₄ samples

Composition	Element	[wt.%]	[at.%]
x = 0.0	O	27.74	55.14
	Al	10.08	11.88
	Fe	32.82	18.68
	Ni	0.47	0.26
	Zn	28.89	14.05
	Total	100	99.81
x = 0.2	O	27.95	56.33
	Al	7.29	8.71
	Fe	22.97	13.27
	Ni	19.35	10.63
	Zn	22.44	11.07
	Total	100	100.01
x = 0.4	O	25.22	53.04
	Al	7.24	9.03
	Fe	21.43	12.91
	Ni	22.07	12.65
	Zn	24.04	12.37
	Total	100	100
x = 0.6	O	21.91	47.00
	Al	12.31	15.66
	Fe	14.55	8.94
	Ni	25.43	14.86
	Zn	25.80	13.54
	Total	100	100
x = 0.8	O	22.12	49.11
	Al	13.98	12.41
	Fe	16.61	12.90
	Ni	23.16	13.44
	Zn	24.13	12.14
	Total	100	100
x = 1.0	O	31.50	60.18
	Al	8.21	9.30
	Fe	16.81	9.20
	Ni	18.59	9.68
	Zn	24.89	11.64
	Total	100	99.81

ration magnetization, remanent magnetization and magnetic moment decrease with increasing Ni²⁺ ion concentration. The observed decrease of the saturation magnetization might be due to lesser magnetic moment of Ni²⁺ ions as compared to that of Fe³⁺ ions and the size-effect. Crystallite size and saturation magnetization are directly related, hence, decreasing the crystallite size indicates the decrease in the saturation magnetization

Table 3. Saturation magnetization (M_S), remanent magnetization (M_R), coercive field (H_C), magnetic moment (μ_B) and molecular weights (M) of Ni_xZn_{1-x}AlFeO₄ (x = 0.0, 0.2, 0.4, 0.6, 0.8 and 1.0) ferrite nanoparticles at room temperature

Composition (x)	M _S [emu/g]	M _R [emu/g]	H _C [kOe]	μ _B	M [g/mol]
0.0	1.3	0.03	395	0.049	212.15
0.2	10.6	0.27	48	0.400	210.81
0.4	9.3	0.26	58	0.348	209.48
0.6	8.8	0.19	40	0.328	208.15
0.8	8.7	0.17	39	0.322	206.82
1.0	4.3	0.42	166	0.158	205.49

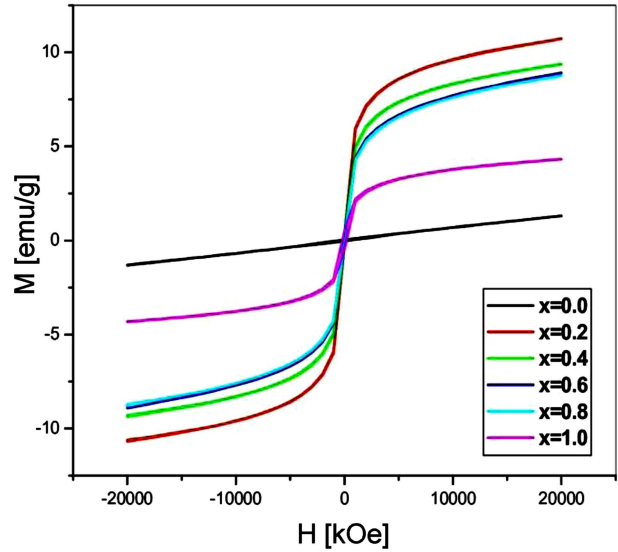


Figure 5. M-H loops of Ni_xZn_{1-x}AlFeO₄ (x = 0.0, 0.2, 0.4, 0.6, 0.8 and 1.0) ferrite nanoparticles

[31]. The observed decrease of saturation magnetization with increasing the Ni²⁺ ion concentration may also be explained by the presence of lattice defects, feeble magnetic super-exchange interaction between tetrahedral and octahedral sites and random orientation of spin on the nanoparticle surfaces [32,33]. Normally, there is a huge difference in the magnetization values between nano-ferrites and bulk ferrites [34], which can be attributed to the finite size effects [35]. The decrease of saturation magnetization in nanoparticles can be attributed to the canted spins in the surface layers due to a decrease in the coupling exchange, which is caused by the lack of oxygen mediating super exchange mechanism between the nearest iron ions at the surface [36]. They can also be attributed to the improvement of the surface barrier potential due to the distortion of crystal lattice caused by the deviation of the atoms from normal positions in the surface layers [37].

Increasing the Ni²⁺ ion concentration together with Al³⁺ ion substitution considerably lowers the saturation magnetization and leads to superparamagnetic behaviour. In our earlier work, we have observed superparamagnetism for the composition of Ni_{0.5}Zn_{0.5}Al_xFe_{2-x}O₄ at x = 2.0 [38].

The coercivity (H_C) is found to vary with increasing the Ni²⁺ ion concentration. The change in the co-

ercivity may be explained by differences in ferrite microstructure, magnetic domain size, particle size and anisotropy [39]. The magnetic moment of the prepared ferrite nanoparticles was found to decrease with increasing the Ni^{2+} ion concentration. This is due to the difference between Neel's theoretical and experimental Bohr magnetic moments which confirms the existence of a non-collinear or canted spin structure that exists in octahedral (B) sites [40,41].

IV. Conclusions

$\text{Ni}_x\text{Zn}_{1-x}\text{AlFeO}_4$ ($x = 0.0, 0.2, 0.4, 0.6, 0.8$ and 1.0) ferrite nanoparticles were synthesized by sol-gel auto combustion technique. XRD results confirmed the formation of single phase spinel cubic structure. The crystallite size and lattice constant were found to decrease from 46 to 15 nm and from 8.334 to 8.281 Å, respectively, with increasing the Ni^{2+} ion concentration. SEM analysis confirmed the nanocrystalline nature, but in the same time the presence of large agglomerated particles. From FTIR spectrum two fundamental bands ν_1 and ν_2 around 600–400 cm^{-1} were observed, that are the common features of all ferrite materials. The characteristic peaks of Ni, Zn, Al, Fe and O elements were observed in EDX spectra, confirming the presence of all constituting elements in the prepared ferrite nanoparticles. Magnetic hysteresis loops were obtained at room temperature by vibrating sample magnetometer. Magnetic measurements confirmed that the saturation magnetization, remanent magnetization and magnetic moment decreased with increasing Ni^{2+} ion concentration in $\text{Ni}_x\text{Zn}_{1-x}\text{AlFeO}_4$ ferrite nanoparticles. Increasing Ni^{2+} ion concentration together with Al^{3+} ion substitution considerably lowers the saturation magnetization and leads to superparamagnetism. Hence, the Ni-Zn-Al mixed nanoferrite particles with the lower saturation magnetization may be suitable for broad range of frequency applications and magnetic recording.

Acknowledgements: The authors DP and PVR are grateful to the Executive Director, SNIST, Ghatkesar, Hyderabad for his support. The author KVK is thankful to Prof. N.V. Ramana, Principal, JNTUH CE, Nachupally (Kondagattu), Karimnagar Dist., TS, India for his constant encouragement in bringing out this research work.

References

1. M.A. Gabal, Y.M. AlAngari, "Effect of chromium ion substitution on the electromagnetic properties of nickel ferrite", *Mater. Chem. Phys.*, **118** (2009) 153–160.
2. D.R. Sharma, R. Mathur, S.R. Vadera, N. Kumar, T.R.N. Kutty, "Synthesis of nano composites of Ni-Zn ferrite in aniline formaldehyde copolymer and studies on their pyrolysis products", *J. Alloys Compd.*, **358** (2003) 193–204.
3. R.C. Kambale, N.R. Adhate, B.K. Chougale, Y.D. Kolekar, "Magnetic and dielectric properties of mixed spinel Ni-Zn ferrites synthesized by citrate nitrate combustion method", *J. Alloys Compd.*, **49** (2010) 372–377.
4. S. Polarz, F. Neues, M.W. Van den Berg, W. Grunert, L. Khodeir, "Mesosynthesis of ZnO-silica composites for methanol nano catalysis", *J. Am. Chem. Soc.*, **127** [34] (2005) 2028–2034.
5. S. Sharma, K. Verma, U. Chaubey, V. Singh, B.R. Mehta, "Influence of Zn substitution on structural, micro structural and dielectric properties of nanocrystalline nickel ferrites", *Mater. Sci. Eng. B*, **167** (2010) 187–192.
6. A.E. Virden, K. O'Grady, "Structure and magnetic properties of Ni-Zn ferrite nanoparticles", *J. Magn. Magn. Mater.*, **290** (2005) 868–870.
7. M. Hashim, S. Kumar, S. Ali, B.H. Koo, H. Chung, R. Kumar, "Structural, magnetic and electrical properties of Al^{3+} substituted Ni-Zn ferrite nanoparticles", *J. Alloys Compd.*, **511** [1] (2012) 107–114.
8. A.M.M. Farea, S. Kumar, K.M. Batoo, A. Yousef, C.G. Lee, "Influence of the doping of Ti^{4+} ions on electrical and magnetic properties of $\text{Mn}_{1+x}\text{Fe}_{2-2x}\text{Ti}_x\text{O}_4$ ferrite", *J. Alloys Compd.*, **469** [1] (2009) 451–457.
9. S.B. Waje, M. Hashim, W.D.W. Yusoff, Z. Abbas, "Sintering temperature dependence of room temperature magnetic and dielectric properties of $\text{Co}_{0.5}\text{Zn}_{0.5}\text{Fe}_2\text{O}_4$ prepared using mechanically alloyed nanoparticles", *J. Magn. Magn. Mater.*, **322** [6] (2010) 686–691.
10. A.C.F.M. Costa, V.J. Silva, D.R. Cornejo, M.R. Morelli, R.H.G.A. Kiminami, L. Gama, "Magnetic and structural properties of NiFe_2O_4 ferrite nano powder doped with Zn^{2+} ", *J. Magn. Magn. Mater.*, **320** [14] (2008) 370–372.
11. S.R. Jain, K.C. Adiga, V.R.P. Vernecker, "A new approach to thermo chemical calculations of condensed fuel-oxidizer mixtures", *Combust. Flame*, **40** (1981) 71–79.
12. J. Smit, H.P.J. Wijn, *Ferrites: Physical Properties of Ferrimagnetic Oxides in Relation to their Technical Applications*. Ed. N.V. Philips Gloeilampenfabrieken, Holland, Eindhoven, 1959.
13. B.D. Cullity, *Elements of X-ray Diffraction*, 2nd ed. Addison-Wesley, Reading, MA, 1978.
14. G.S. Shahane, A. Kumar, M. Arora, R.P. Pant, K. Lal, "Synthesis and characterization of Ni-Zn ferrite nanoparticles", *J. Magn. Magn. Mater.*, **322** (2010) 1015–1019.
15. A.A. El-Sayed, "Influence of zinc content on some properties of Ni-Zn ferrites", *Ceram Int.*, **28** (2002) 363–367.
16. A.T. Raghavender, N. Biliskov, Z. Skoko, "XRD and IR analysis of nanocrystalline Ni-Zn ferrite synthesized by the sol-gel method", *Mater. Lett.*, **65** (2011) 677–680.

17. M. Popovici, C. Savii, D. Niznansky, J. Subrt, J. Bohacek, D. Becherescu, C. Caizer, C. Enache, C. Ionescu, “Nanocrystalline Ni-Zn ferrites prepared by sol-gel method”, *J. Optoelectron. Adv. Mater.*, **5** (2003) 251–256.
18. I.H. Gul, W. Ahmed, A. Maqsood, “Electrical and magnetic characterization of nanocrystalline Ni-Zn ferrite synthesis by co-precipitation route”, *J. Magn. Magn. Mater.*, **320** [3] (2008) 270–275.
19. R. Sharma, S. Singhal, “Structural, magnetic and electrical properties of zinc doped nickel ferrite and their application in photo catalytic degradation of methylene blue”, *Physica B*, **414** (2013) 83–90.
20. K. Rama Krishna, K. Vijaya Kumar, D. Ravinder, “Structural and electrical conductivity studies in nickel-zinc ferrite”, *Adv. Mater. Phys. Chem.*, **2** (2012) 185–191.
21. R.D. Waldron, “Infrared spectra of ferrites”, *Phys. Rev.*, **99** (1955) 1727.
22. M.M. Mallapur, P.A. Shaikh, R.C. Kambale, H.V. Jamadar, P.U. Mahamuni, B.K. Chougule, “Structural and electrical properties of nanocrystalline cobalt substituted nickel zinc ferrite”, *J. Alloys Compd.*, **479** [1] (2009) 797–802.
23. R.C. Kambale, K.M. Song, Y.S. Koo, N. Hur, “Low temperature synthesis of nanocrystalline Dy³⁺ doped cobalt ferrite, structural and magnetic properties”, *J. Appl. Phys.*, **110** [5] (2011) 053910–053917.
24. M.A. Gabal, Y.M. Al Angari, “Low-temperature synthesis of nanocrystalline Ni-Cu-Zn ferrite and the effect of Cr substitution on its electrical properties”, *J. Magn. Magn. Mater.*, **322** [20] (2010) 3159–3165.
25. S. Zahi, “Synthesis, permeability and microstructure of the optimal nickel-zinc ferrites by sol-gel route”, *J. Electromagn. Anal. Appl.*, **2** (2010) 56–62.
26. T.K. Pathak, N.H. Vasoya, V.K. Lakhani, K.B. Modi, “Structural and magnetic phase evolution study on needle-shaped nanoparticles of magnesium ferrite”, *Ceram. Int.*, **36** [1] (2010) 275–281.
27. M. Vijatovic Petrovic, J. Bobic, H. Ursic, J. Banys, B. Stojanovic, “The electrical properties of chemically obtained barium titanate improved by attrition milling”, *J. Sol-Gel Sci. Technol.*, **67** (2013) 267–272.
28. A. Verma, R. Chatterjee, “Effect of zinc concentration on the structural, electrical and magnetic properties of mixed Mn-Zn and Ni-Zn ferrites synthesized by the citrate precursor technique”, *J. Magn. Magn. Mater.*, **306** [2] (2006) 313–320.
29. E. Pervaiz, I.H. Gul, “Low temperature synthesis and enhanced electrical properties by substitution of Al³⁺ and Cr³⁺ in Co-Ni nanoferrites”, *J. Magn. Magn. Mater.*, **343** (2013) 194–202.
30. M.A. Gabal, R.M. El-Shishtawy, Y.M. Al Angari, “Structural and magnetic properties of nanocrystalline Ni-Zn ferrites synthesized using egg-white precursor”, *J. Magn. Magn. Mater.*, **324** [14], (2012) 2258–2264.
31. A.C.F.M. Costa, E. Tortella, M.R. Morelli, R.H.G.A. Kiminami, “Synthesis, microstructure and magnetic properties of Ni-Zn ferrites”, *J. Magn. Magn. Mater.*, **256** [1] (2003) 174–182.
32. K.H. Wu, T.H. Ting, G.P. Wang, C.C. Yang, B.R. Mc Garvey, “EPR and SQUID studies on magnetic properties of SiO₂-doped Ni-Zn ferrite nano composites”, *Mater. Res. Bull.*, **40** [12] (2005) 2080–2088.
33. B.P. Rao, A. Mahesh Kumar, K.H. Rao, Y.L.N. Murthy, O.F. Caltun, I. Dumitru, L. Spinu, “Synthesis and magnetic studies of Ni-Zn ferrite nanoparticles”, *J. Optoelectron. Adv. Mater.*, **8** (2006) 1703–1705.
34. A.A.K.M. Hossain, S.T. Mahmud, M. Seki, T. Kawai, H. Tabata, “Structural, electrical transport, and magnetic properties of Ni_{1-x}Zn_xFe₂O₄”, *J. Magn. Magn. Mater.*, **312** [1] (2007) 210–219.
35. W. Yan, W. Jiang, Q. Zhang, Y. Li, H. Wang, “Structure and magnetic properties of nickel-zinc ferrite microspheres synthesized by solvothermal method”, *Mater. Sci. Eng. B*, **171** [1] (2010) 144–148.
36. L.R. Penn, “Kinetics of oriented aggregation”, *J. Phys. Chem. B*, **108** [34] (2004) 12707–12712.
37. B. Jia, L. Gao, “Growth of well-defined cubic hematite single crystals: oriented aggregation and Ostwald ripening”, *Crystal Growth Design*, **8** [4] (2008) 1372–1376.
38. K. Vijaya Kumar, D. Paramesh, P. Venkat Reddy, “Effect of aluminium doping on structural and magnetic properties of Ni-Zn ferrite nanoparticles”, *World J. Nano Sci. Eng.*, **5** (2015) 68–77.
39. J. Jing, L. Li, X. Feng, “Structural analysis and magnetic properties of Gd-doped Li-Ni ferrites prepared using rheological phase reaction method”, *J. Rare Earths*, **25** [1] (2007) 79–83.
40. S. Sharma, N.D. Sharma, “Mossbauer, X-ray and magnetization studies of ZnAl_xFe_{2-x}O₄ system”, *Indian J. Pure Appl. Phys.*, **44** [3] (2006) 220–226.
41. M.M. Eltabey, K.M. El-Shokrofy, S.A. Gharbia, “Enhancement of the magnetic properties of Ni-Cu-Zn ferrites by the non-magnetic Al³⁺ ions substitution”, *J. Alloys Compd.*, **509** [5] (2011), 2473–2477.

